Research article

Spatial distribution of degradation and deforestation of palm swamp peatlands and associated carbon emissions in the Peruvian Amazon

Matthew S. Marcus [a,e,*], Kristell Hergoualc'h [b,d], Eurídice N. Honorio Coronado [c], Víctor Hugo Gutiérrez-Vélez [a]

[a] Temple University, Department of Geography and Urban Studies, Philadelphia, PA, USA
[b] Center for International Forestry Research (CIFOR), Lima, Peru
[c] School of Geography and Sustainable Development, University of St Andrews, St Andrews, KY16 9AL, United Kingdom
[d] Centre de coopération International en Recherche Agronomique pour le Développement (CIRAD), UMR Eco&Sols, Montpellier, France
[e] University of Arizona, School of Geography, Development and Environment, Tucson, AZ, USA

ABSTRACT

The vast peat deposits in the Peruvian Amazon are crucial to the global climate. Palm swamp, the most extensive regional peatland ecosystem faces different threats, including deforestation and degradation due to felling of the dominant palm Mauritia flexuosa for fruit harvesting. While these activities convert this natural C sink into a source, the distribution of degradation and deforestation in this ecosystem and related C emissions remain unstudied. We used remote sensing data from Landsat, ALOS-PALSAR, and NASA's GEDI spaceborne LiDAR-derived products to map palm swamp degradation and deforestation within a 28 Mha area of the lowland Peruvian Amazon in 1990–2007 and 2007–2018. We combined this information with a regional peat map, C stock density data and peat emission factors to determine (1) peatland C stocks of peat-forming ecosystems (palm swamp, herbaceous swamp, pole forest), and (2) areas of palm swamp peatland degradation and deforestation and associated C emissions. In the 6.9 ± 0.1 Mha of predicted peat-forming ecosystems within the larger 28 Mha study area, 73% overlaid peat (5.1 ± 0.9 Mha) and stored 3.88 ± 0.12 Pg C. Degradation and deforestation in palm swamp peatlands totaled $535,423 \pm 8,419$ ha over 1990–2018, with a pronounced dominance for degradation (85%). The degradation rate increased 15% from 15,400 ha y^{-1} (1990–2007) to 17,650 ha y^{-1} (2007–2018) and the deforestation rate more than doubled from 1,900 ha y^{-1} to 4,200 ha y^{-1}. Over 1990–2018, emissions from degradation amounted to 26.3 ± 3.5 Tg C and emissions from deforestation were 12.9 ± 0.5 Tg C. The 2007–2018 emission rate from both biomass and peat loss of 1.9 Tg C yr^{-1} is four times the average biomass loss rate due to gross deforestation in 2010–2019 reported for the hydromorphic Peruvian Amazon. The magnitude of emissions calls for the country to account for deforestation and degradation of peatlands in national reporting.

Author contributions statement

Matthew Marcus: Methodology, Software, Validation, Investigation, Formal analysis, Resources, Writing – original draft, Visualization; Kristell Hergoualc'h: Conceptualization, Formal analysis, Writing – review & editing, Supervision, Project administration, Funding acquisition; Eurídice N. Honorio Coronado: Writing – review & editing; Víctor Hugo Gutiérrez-Vélez: Methodology, Formal analysis, Investigation, Writing – review & editing, Supervision

1. Introduction

The lowland Peruvian Amazon has been revealed to contain vast carbon (C) deposits of peat (Lähteenoja et al., 2012; Draper et al., 2014; Hastie et al., 2022). Peat forms in (quasi-) permanently waterlogged environments where organic matter degrades slowly accumulating in large reservoirs of C over the timescale of millennia (Petrescu et al., 2015; Flores Llampazo et al., 2022). However, if disturbed, peat soils lose C and can become large sources of CO_2 (Limpens et al., 2008; Lähteenoja et al., 2009b; Wang et al., 2018), and N_2O (Drösler et al.,

2014; Swails et al., 2021) owing to the stimulation of soil organic matter decomposition, changes in the amount and nature of litter inputs and modifications in the environment (van Lent et al., 2019; Hergoualc'h et al., 2020). Disturbance of the vegetation also leads to biomass losses and associated CO_2 emissions.

Hastie et al. (2022) mapped 6.3 million ha (Mha) of peatlands within 78 Mha of the lowland Peruvian Amazon in the departments of Loreto, Ucayali and Madre de Dios. These peatlands form on floodplains of major rivers and in geomorphological features that favor waterlogged conditions (Kalliola et al., 1991). In total, the region was estimated to store 5.4 PgC in peat soil which is nearly the entire above-ground carbon stock of Peru (Hastie et al., 2022). For context, the Peruvian peatlands are one of the largest deposits of peat in the tropics, however they are smaller than the peatlands of Southeast Asia, which contain an estimated 68.5 PgC, and the peatlands of the Congo basin, which contain an estimated 30.6 PgC (Cole et al., 2022). The highest concentration of peatlands occurs in the Pastaza-Marañón foreland basin (PMFB) in the Loreto department (Draper et al., 2014; Gumbricht et al., 2017). This basin has accumulated peat deposits up to 7.5 m thick (Lähteenoja et al., 2012) and holds 76% of the estimated peat C stock in the lowland Peruvian Amazon (Hastie et al., 2022).

Palm swamp is the most extensive peat-forming ecosystem covering an estimated 4.6 Mha across the lowland Peruvian Amazon (Hastie et al., 2022). Palm swamps are an important source of livelihood for many people throughout the region by providing income from fruit sales, and also deliver critical ecosystem services, such as food, water flux regulation, and hunting grounds (Gilmore et al., 2013; Virapongse et al., 2017; Schultz et al., 2019). The palm *M. flexuosa* is considered a "hyperkeystone" species (van der Hoek et al., 2019) and contributes to peat formation by producing vegetation litter both above and belowground (Dezzeo et al., 2021). *M. flexuosa* is dioecious, meaning that individual palms are either males (pollen producers) or females (fruit producers) (Holm et al., 2008). Among numerous anthropogenic threats, palm swamps have been degraded by the destructive method of harvesting *M. flexuosa* fruit by felling female individuals (Penn, 2008; Horn et al., 2018). Horn et al. (2018) estimated that between 2012 and 2013 approximately 114,000 palms were felled. As a result, *M. flexuosa* abundance and density decrease in increasingly degraded sites (Horn et al., 2012; Hidalgo Pizango et al., 2022) and become more male-dominated which reduces the capacity of the species to reproduce (Virapongse et al., 2017; Falen Horna and Honorio Coronado, 2018). Consequences include a reduction in biomass and necromass C stocks and in litter C inputs which build up the peat over time (Hergoualc'h et al., 2017; Bhomia et al., 2019; Dezzeo et al., 2021; Hergoualc'h et al., 2023). Depending on the intensity of degradation the natural C sink capacity of the soil can be reduced, or the soil can turn into a C source (van Lent et al., 2019; Hergoualc'h et al., 2020). CO_2 emissions from degraded peatlands have been documented in Indonesia, following conversion to oil palm and pulpwood production (Murdiyarso et al., 2019).

Despite the environmental, social, and economic importance of palm swamps to rural communities, little is known about the magnitude and spatial distribution of degradation and deforestation occurring in this ecosystem. To date, studies have focused on mapping ecosystem types for the Peruvian Amazon (MINAM, 2015), peat-forming ecosystems at the regional scale within the departments of Loreto (Draper et al., 2014; Honorio Coronado et al., 2021), Ucayali (Revilla-Chavez et al., 2019) and Madre de Dios (Householder et al., 2012), and ecosystems and peat thickness throughout the entire lowland Peruvian Amazon (Hastie et al., 2022). A map of *M. flexuosa* stands under different levels of degradation is also available, at the local scale and for a single date (Hergoualc'h et al., 2017). Based on national data, Bourgeau-Chavez et al. (2021) and Hastie et al. (2022) found low deforestation rates within peatlands, due mainly to conversion to agriculture and pasture, however mining, oil drilling activities and new road construction were also identified as potential drivers of deforestation and degradation in the region

(Householder et al., 2012; Roucoux et al., 2017; Lawson et al., 2022). Hastie et al. (2022) detected increasing deforested areas on peatlands from 2000 to 2016 which generated peat emissions of 4.4 TgC or about 3% of biomass emissions from gross deforestation in the lowland Peruvian Amazon. Yet, the magnitude of palm swamp peatland loss due to both degradation and deforestation and the associated carbon emissions remain unassessed.

Given the existing threats on palm swamps and current limited knowledge of their conservation status, this paper aimed to characterize the degradation and deforestation of palm swamp peatlands in the lowland Peruvian Amazon and to estimate associated carbon emissions. Our three main goals were (1) to map peat-forming ecosystems (herbaceous swamp, *Mauritia flexuosa* palm swamps, pole forest) and quantify their C stock where they overlay peat, (2) to map palm swamp peatland degradation and deforestation over the periods 1990–2007 and 2007–2018 and (3) to quantify resulting CO_2–C emissions from both vegetation and soil losses.

2. Methods

2.1. Study area and workflow

The study was conducted in peatland-dominated areas in the lowland Peruvian Amazon within the basins of the Ucayali, Marañón, Napo, and Amazon Rivers in the Loreto and Ucayali regions (Fig. 1). The study area covers 28 Mha, including 6.2 Mha (out of 6.3 Mha) of the peatlands (Hastie et al., 2022) and encompasses the full region of *M. flexuosa* fruit extraction (Horn et al., 2018). Local climate is described in SI Methods 1. Three major peat-forming wetland types were identified by Draper et al. (2014) in the PMFB: palm swamp, open peatland (here referred to as herbaceous swamp), and pole forest. Palm swamps form in low-lying areas over mostly minerotrophic peat and are dense in *Mauritia flexuosa* (Lähteenoja et al., 2009a; Bhomia et al., 2019), a palm species that typically dominates the canopy reaching heights of 35–40 m (Draper et al., 2014). Pole forests grow on ombrotrophic domes, and usually sit atop large deposits of peat (ibid.). Ombrotrophic environments cause trees to grow relatively short, thin stemmed, and in dense patches, with *M. flexuosa* occurring at low densities (Draper et al., 2018; Honorio Coronado et al., 2021). Herbaceous swamps are characterized by sedges and grasses, with scattered trees and *M. flexuosa* palms (Lähteenoja and Page, 2011). Palaeoecological studies suggest that herbaceous swamp is an early successional state of a palm swamp, and pole forest represents a late successional state (Roucoux et al., 2013; Kelly et al., 2017, 2020; Swindles et al., 2017). Although these ecosystems have the capacity to accumulate peat, they can also occur over mineral soils, especially in the case of palm swamps (Freitas Alvarado et al., 2006; Honorio Coronado et al., 2021). Similar vegetation physiognomy to pole forests occur on mineral white sand soils (Fine et al., 2010) and can be confused with the forest structure of pole forest but this ecosystem type is more related to terra firme formations (Draper et al., 2018; Palacios et al., 2016). Finally, seasonally flooded forest is dominated by trees and scarce palms and can occasionally be underlain by peat, however peat has only been predicted in 2% of this extensive wetland ecosystem type in lowland Peruvian Amazonia (Hastie et al., 2022).

The research entailed several steps which are presented in Fig. 2. Briefly, we produced ecosystem maps for the region in the years 1990, 2007 and 2018, using remote sensing data. We further filtered the classifications with the Hastie et al. (2022) peat map, and computed total C stocks of peat-forming ecosystems (herbaceous swamp, palm swamp, pole forest) in 2018. Then we analyzed changes over time in palm swamp peatlands over the periods 1990–2007 and 2007–2018 and estimated C emissions resulting from degradation and deforestation.

2.2. Remote sensing image sources and pre-processing

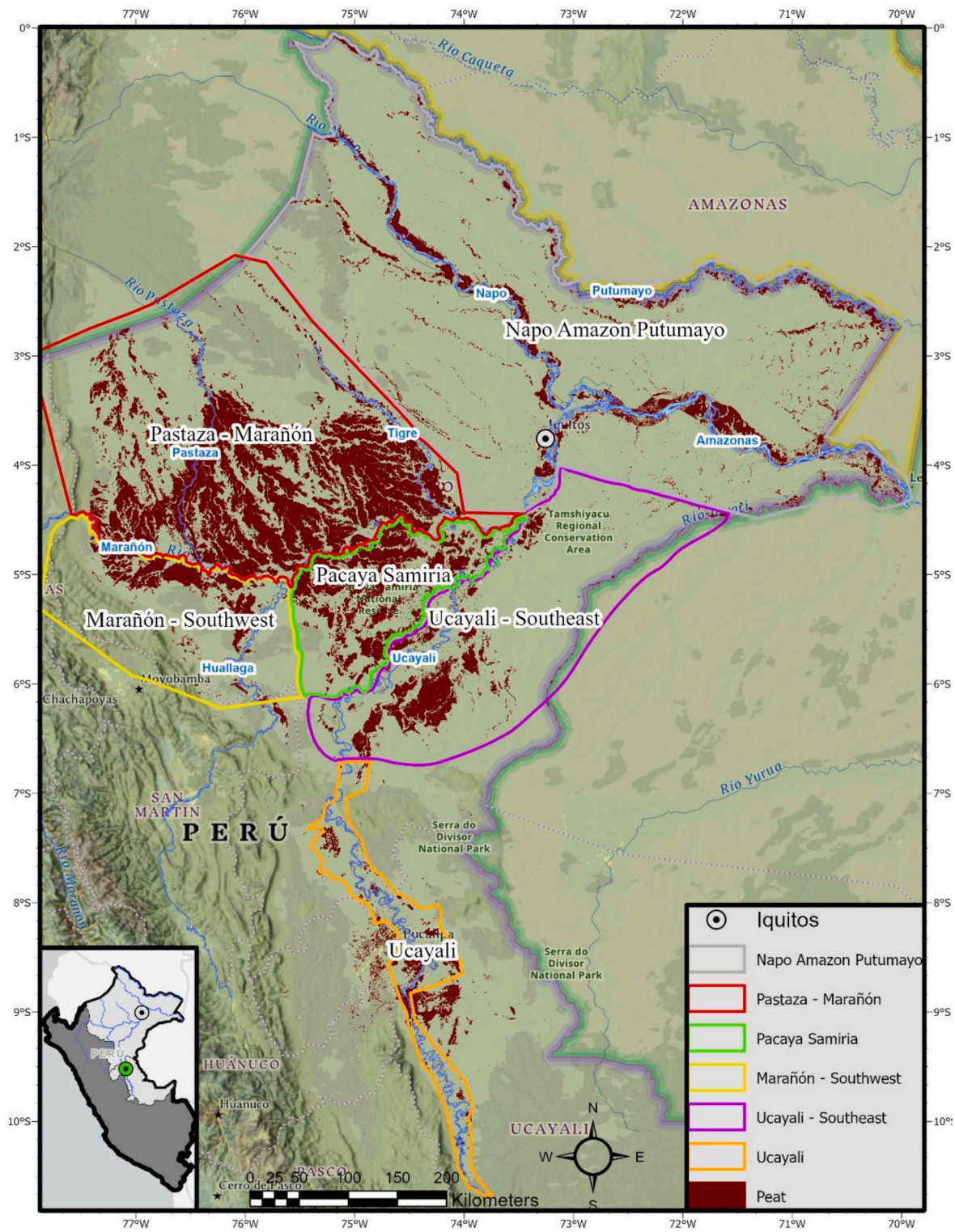A stack of different remote sensing layers was created for each of 3

Fig. 1. Study area showing peatlands (brown) according to Hastie et al. (2022). Six geographical areas were delineated for results description. (For interpretation of the references to colour in this figure legend, the reader is referred to the Web version of this article.)

landcover classifications for the years 2018, 2007, and 1990. The 2018 and 2007 mosaics were constructed using Analysis Ready Data (ARD) from the Global Land Analysis and Discovery (GLAD) laboratory. ARD is a global Landsat based dataset containing cloud-free, error corrected, and radiometrically normalized remotely sensed data which do not require preprocessing and are delivered in a full mosaic (Potapov et al., 2020). Given the absence of ARD data from before 1997, we constructed

the 1990 mosaic using single-date Landsat images. To classify the 1990 image, we applied an algorithm that was calibrated using the same training data applied to the ARD mosaics on a manually-produced mosaic for 2018 from single-date images. Single-date Landsat 1990 and 2018 images (at the collection 1, level 2 processing, representing ground reflectance) were acquired from the United States Geologic Survey's (USGS) website (earthexplorer.gov) for constructing the
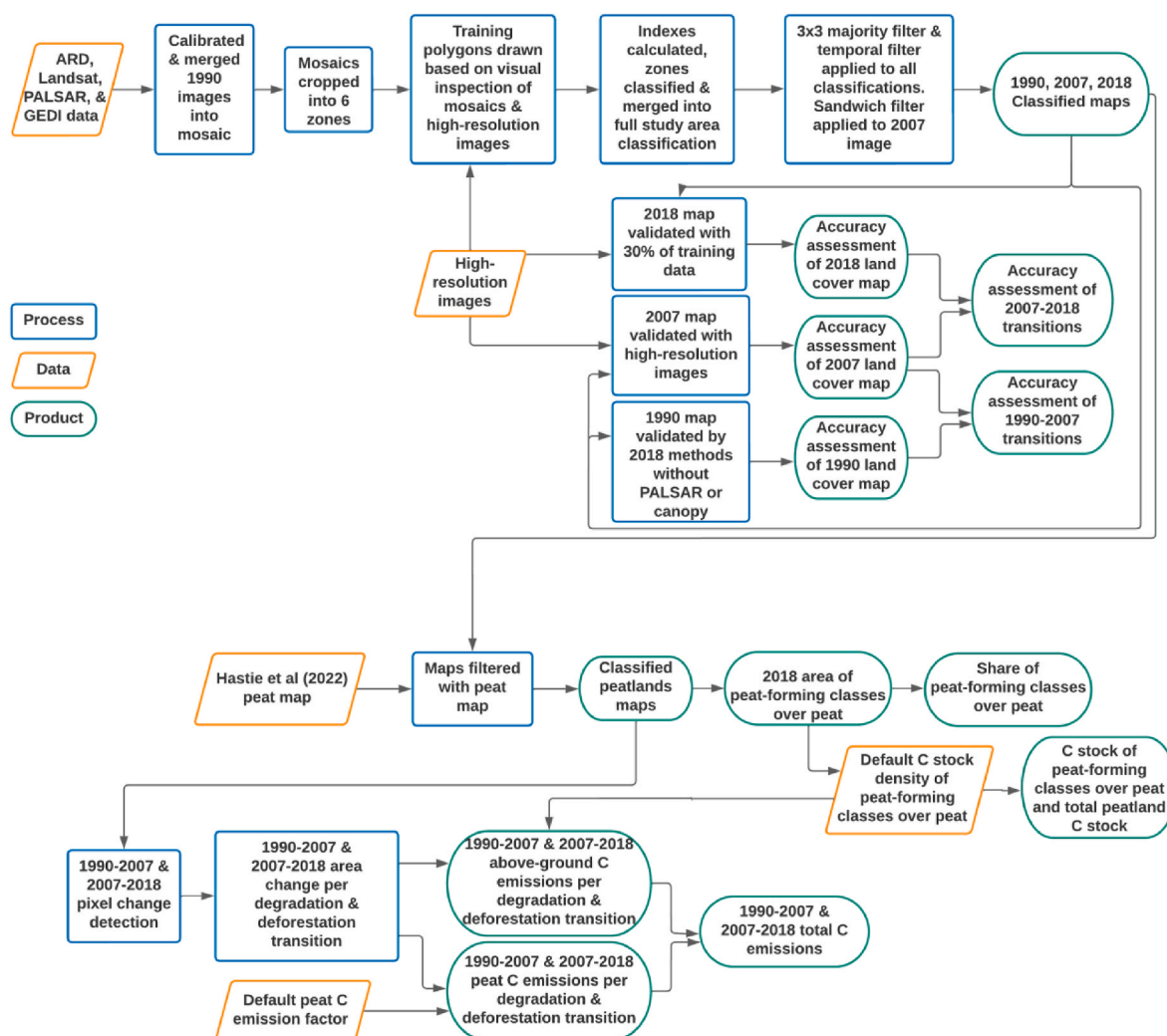
Fig. 2. Workflow leading to the assessment of peatland area and C stock in 2018, and of degraded and deforested areas and associated C emissions between 1990 and 2018 in the Peruvian Amazon.

manually-produced mosaics. Landsat bands used in the classifications included the red, green, NIR, SWIR1 and SWIR2, and three spectral indices derived from them (NDVI, NDWI, and MSAVI). Other bands include 2 from ALOS-PALSAR (HH and HV polarizations). In addition, a layer of forest canopy height (derived from GEDI LiDAR data) was used in the 2018 classification to help distinguish between forest ecosystems of different vegetation structure (SI Methods 2).

Then, training data was collected over multiple high-resolution images across the study area, which were used to draw 1,444 polygons including the following peat-forming classes: palm swamp, herbaceous swamp, and pole forest; and for the following non-peat-forming classes: seasonally flooded forest, *terra firme* forest, pasture, lake, river, sand bank, secondary forest, and urban areas (Table SI 4). The lake and river classes were merged to form a water class; otherwise, the aforementioned classes form the classification output. The palm swamp class was disaggregated by density of *M. flexuosa* palms. Low density was defined as a swamp with a canopy consisting of less than one-third of *M. flexuosa* where crowns never overlapped (Figure SI 2A). Medium density was defined as a canopy consisting of approximately one to two-thirds of *M. flexuosa* with canopy breaks including other vegetation, both herbaceous vegetation and trees (Figure SI 2B). High density was defined as a swamp with an unbroken canopy dominated almost entirely by *M. flexuosa* individuals (Figure SI 2C). SI Methods 2–5 present more detail on the classification process and the input spatial products used

for classification are reported in Table SI 3.

2.3. Classification, accuracy assessment, area, and area uncertainty estimation

A supervised random forest classification was performed for each year and was trained with 70% of the training polygons. Classification accuracy for the years 2018 and 2007 was assessed from the comparison of classes to the 30% of the training polygons unused for classification (Olofsson et al., 2014). The 1990 classification was produced by training a random forest model on the 2018 manually-produced mosaic (composed of single date Landsat scenes), and then using the produced random forest to predict land cover classes for the 1990 mosaic. We estimated the accuracy of the 1990 map by validating the 2018 manually-produced mosaic with the same validation polygons used for the 2018 accuracy assessment. This was done because high resolution imagery was not available in 1990, and so validation data could not be acquired for this year. The 2018 manually-produced mosaic and the 1990 mosaic contained the same spectral bands and were normalized to a common standard, allowing for the accuracy assessment of the 2018 manually-produced mosaic's classification to represent the accuracy of the 1990 classification. All classifications had a resolution of 30m.

The accuracy assessment was performed by converting the error matrix into values based on the proportion of area mapped for each class

(Olofsson et al., 2014; Stehman and Foody, 2019). We assessed both producer's and user's accuracy. Producer's accuracy refers to the accuracy from the perspective of the map maker. It assesses how well a land cover observed on the ground is also represented in the map. User's accuracy refers to the perspective of a map user on the ground. It assesses how likely a land cover represented in the map is also observed in the field.

For all three classifications (1990, 2007, and 2018), the area of the classes and their uncertainty was estimated based on the error matrix (Olofsson et al., 2014). The area was computed as:

$$\hat{A}_k = A \times \hat{p}_k \qquad (1)$$

Where $\hat{A}_k$ is the estimated area of class k, A is the total map area, and $\hat{p}_k$ is the estimator of the proportion of area of class k computed based on the error matrix (detailed equation provided by Olofsson et al. (2014).

The standard error was computed as:

$$SE_{\hat{A}k} = A \times S(\hat{p}_k)() \qquad (2)$$

Where SE $_{\hat{A}k}$ is the standard error of the estimated area for class k, A is the total map area, and $S(\hat{p}_k)$ is the standard error of the $\hat{p}_k$ estimator computed based on the error matrix (detailed equation provided by Olofsson et al. (2014)). All error matrices are presented in Table SI 8.

Areas and area uncertainties of each class were estimated by multiplying the area proportions of each class, based on the error matrix, by the total mapped area (Olofsson et al., 2014).

2.4. Deforestation and degradation in palm swamp peatlands and peatland area

We evaluated degradation and deforestation based on transitions occurring in palm swamp peatlands (i.e., with classifications filtered with the Hastie et al. (2022) peat map as peat-forming ecosystems occasionally occur over mineral soil (López Gonzales et al., 2020)). The Hastie et al. (2022) peat map was resampled from its native resolution of 100m to 30m before filtering. These transitions were those involving a decrease in palm density as well as conversion of palm swamp into herbaceous swamp. A decrease over time in *M. flexuosa* density was assumed to result from degradation and included the transitions from high density to medium density or from high and medium density to low density. A transition from palm swamp of any density to herbaceous swamp was assumed to result from deforestation rather than from a natural process which would take place on timescales much longer than one or two decades.

Accuracy was calculated for all degradation and deforestation transitions (Glinskis and Gutierrez-Velez, 2019) regardless of the presence of peat (i.e. before filtering land cover classifications with the Hastie et al. (2022) map. The accuracy of a pixel transitioning from one class to another was equal to the product of the accuracies of the classes assigned to it before and after transition, for both producer's and user's accuracies.

We assessed the area of peatlands based on the 2018 classification filtered with the Hastie et al. (2022) peat map using the assumption that only peat-forming ecosystems (palm swamp, herbaceous swamp, and pole forest) occur over peat. This approach differs slightly from the one undertaken by Hastie et al. (2022) who put no constraint on ecosystem type over peat.

The area of a peat-forming class over peat was computed as:

$$\hat{A}_{k\,peat} = (A_{k\,peat} \,/\, A_k) \times \hat{A}_k \qquad (3)$$

Where $\hat{A}_{k\,peat}$ is the estimated area of class k over peat, $\hat{A}_k$ is the estimated area of class k (Eq. (1)), $A_{k\,peat}$ and A_k are, respectively, the mapped area of class k after and before filtering with the Hastie et al. (2022) peat map based on a pixel count.

The standard error per class was computed as:

$$SE_{\hat{A}k\,peat} = (A_{k\,peat} \,/\, A_k) \times SE_{\hat{A}k} \qquad (4)$$

Where SE $_{\hat{A}k\,peat}$ is the standard error of the estimated area of class k over peat, and SE $_{\hat{A}k}$ is the standard error of the estimated area for class k (Eq. (2)).

Transition areas over peat were estimated by applying a modified version of the area estimation by Olofsson et al. (2014) as:

$$\hat{A}_t = UA_t * A_t \qquad (5)$$

Where $\hat{A}_t$ is the estimated area of the transition over peat, UA_t is the user's accuracy of the transition, and A_t is the area of the transition over peat.

Standard error for each transition occurring over peat was calculated as:

$$SE_{\hat{A}k,\hat{A}l\,peat} = A_t * ((SE_{\hat{A}k\,peat} \,/\, \hat{A}_{k\,peat} + (SE_{\hat{A}l\,peat} \,/\, \hat{A}_{lpeat}) \qquad (6)$$

Where SE $_{\hat{A}k,\hat{A}l\,peat}$ is the standard error for the transition from class k to class l over peat, A_t is the area of the transition, SE $_{\hat{A}k\,peat}$ is the standard error of class k over peat (Eq. (4)), $\hat{A}_{k\,peat}$ is the estimated area of class k over peat (Eq. (3)), SE $_{\hat{A}l\,peat}$ is the standard error of class l over peat, and $\hat{A}_{l\,peat}$ is the estimated area of class l over peat.

Rates of degradation and deforestation are presented at the scale of the entire study area as well as per geographical areas to inspect local variations. We delineated 6 areas within the landscape; from northeast to southwest: Napo Amazon Putumayo, Pastaza – Marañón, Marañón – southwest, Pacaya Samiria, Ucayali – southeast, and Ucayali (Fig. 1). These contiguous, non-overlapping areas present significant socio-ecological differences among them. For example, palm destructive harvest is prohibited in the Pacaya Samiria National Reserve while destructive harvest and oil infrastructure are common in the adjacent Pastaza-Marañon area (Roucoux et al., 2017). Degradation and deforestation extent per geographical area were computed based on the assumption of a homogeneous accuracy of classes and transitions across the landscape as:

$$\hat{A}_{t\,geographical\,area} = A_{t\,geographical\,area} * (\hat{A}_t \,/\, A_t) \qquad (7)$$

Where $\hat{A}_{t\,geographical\,area}$ is the estimated extent of a transition over peat within a geographical area, $A_{t\,geographical\,area}$ is the area of the transition over peat within a geographical area, $\hat{A}_t$ is the estimated area over peat of the transition for the entire study area, and A_t is the area of transition over peat for the entire study area.

2.5. Carbon stock and carbon emissions from degradation and deforestation

Carbon stocks in peatlands were estimated from the areas of peat-forming classes and class-specific C stocks. Default C stocks for the above-ground (AGB) and below-ground biomass (BGB) and the soil were taken directly from published findings in the literature, or were derived from these sources (SI Table 7). For example, AGB in a high-density palm swamp is assumed to have the storage of an undegraded swamp of 75.6 $\pm$ 4.3 Mg C ha^{-1}, as reported in Honorio Coronado et al. (2021), and a medium-density palm swamp is assumed to have 89% the storage of a high-density palm swamp, according to Hergoualc'h et al. (2017).

Carbon emissions from degradation and deforestation were derived from areas of palm swamp peatland transitions and transition-specific C stock changes. Stock changes included the AGB and soil pools only since changes in BGB are indirectly accounted for in peat emission factors (Drösler et al., 2014; Hergoualc'h & Verchot, 2011). AGB losses were computed as the difference of C stock post- and pre-conversion from Table SI 6. Soil CO_2–C losses were calculated from the peat emission or uptake rate multiplied with the time of the transition (1990–2007, 2007–2018). The peat flux rate for each transition was the average of the

emission factor before and after conversion. Whenever the class before conversion was an active C sink, the loss from removing the sink was also accounted for. Peat CO$_2$–C emission factors per class and transition are provided in Table SI 7.

In all C stocks and C emissions calculations, the Gaussian error propagation (GEP) method was used for propagating uncertainties (see SI Methods 6 for details). This method is adequate for step-by-step calculations that are intended to compute ecological quantities that can be expressed as an analytical equation using addition, subtraction, multiplication and division, such as C emissions (Lo, 2005). Uncertainties were propagated by quadrature of absolute errors for addition and subtraction, and quadrature of relative error for multiplication and division (Malhi et al., 2009).

3. Results

3.1. Land cover mapping and peatland C stock

3.1.1. Area of peat-forming classes over peat and distribution of peatland classes in 2018

Peat-forming vegetation covered 6.9 Mha (Table 1). Palm swamp was the most extensive class with a total of 5.5 Mha, followed by pole forest and herbaceous swamp. Peat-forming classes over peat extended across 5.1 Mha with a predominance of palm swamp (4.2 Mha, 83%) over herbaceous swamp and pole forest (7% and 10%, respectively). On average, 73% of peat-forming ecosystem classes overlapped peat, with the lowest percent share for herbaceous swamps (59%). The study area encompassed an important extent of peatlands which did not classify as peat-forming vegetation, notably seasonally flooded forest (776,350 ± 8,550 ha) and terra firme forest (214,660 ± 2,370 ha) (Figure SI 5).

Peatlands were predominant in the north with 81% of their extent located in the Pastaza-Marañón, Napo Amazon Putumayo, and Pacaya Samiria areas. The Ucayali-southeast and Ucayali areas only accounted for 10% of peatlands (Fig. 3b, Table 2).

High density palm swamps were most prominent throughout the Pastaza-Marañón area, and along the Marañón and Huallaga Rivers. Medium and Low density palm swamps were most prominent in the Pastaza-Marañón area, Pacaya-Samiria reserve and Ucayali-southeast (Fig. 3a).

Herbaceous swamps were most common within the Pastaza-Marañón area, between the arc of low-density palm swamps and the Marañón River, along the Pastaza River, near the Ucayali River within Pacaya Samiria, and within the Ucayali-southeast area. The largest growth of pole forests was located within the Pastaza-Marañón area by the Tigre River while other patches were present in some meanders of the Amazon River south of Iquitos, and within meanders of the Napo River (Fig. 3).

Table 1

Total area and area over peat ± SE of peat-forming classes in 2018. The presence of peat was identified using the map by Hastie et al. (2022). HS classified as PS in the years 1990 and 2007 were included in the HS class. PS: Palm swamp, HS: Herbaceous swamp, PF: Pole forest.

Class	Area (ha)	Share over peat (%)	Area over peat (ha)
PS high density	1,597,579 ± 66,382	75	1,198,184 ± 49,787
PS medium density	1,808,226 ± 80,390	85	1,536,992 ± 68,332
PS low density	2,077,066 ± 54,076	70	1,453,946 ± 37,853
HS and HS formerly classified as PS	627,307 ± 3,909	59	370,111 ± 12,563
PF	793,677 ± 20,931	63	500,017 ± 12,534
All	6,903,855 ± 119,360	73	5,059,250 ± 94,317

3.1.2. Classification accuracy assessment of land cover maps

The land cover map in 2018 is presented in Fig. 3a while maps for the years 1990 and 2007 are available in Figure SI 5. The overall accuracy for the entire study area was 87%, 84% and 93% for the years 1990, 2007 and 2018, respectively. Some confusion occurred between palm swamps of different density (Fig. 4a) owing to similar spectral characteristics of these classes. User's accuracy for pole forest was above 75% and herbaceous swamp had the highest accuracy of peat-forming classes (99% user's accuracy, and 96% producer's accuracy). The accuracy of peat-forming and non-peat forming classes were both high (Fig. 4b). All error matrices are presented in SI Table 9.

3.1.3. Peatland C stock in 2018

Peatland C stock amounted to 3.88 ± 0.12 Pg, with palm swamps accounting for the largest portion (79%), followed by pole forest (15%) and herbaceous swamp (6%) (Table 3). The C stock in the peat was one order of magnitude higher as compared to stock in the biomass.

3.2. Palm swamp peatland degradation and deforestation

3.2.1. Accuracy of transitions

The overall accuracy of the 1990–2007 transition and the 2007–2018 transition was 73%, and 78%, respectively (Fig. 5).

3.2.2. Degradation and deforestation in palm swamp peatlands: Distribution, areas and rates

Degradation was considerably more important than deforestation with an area approximately 6 times that of deforestation (Table 4). Of the 4.2 Mha of palm swamp peatland, 11% and 2% were degraded and deforested, respectively by 2018. While the rate of degradation increased by 14% in 2007–2018 compared to 1990–2007, the rate of deforestation raised considerably by 117% (Table 5).

Degradation and deforestation were prominent within the Pastaza-Marañón accounting for 58 and 69% of the total over 1990–2018 (Table 4). Important extents of degradation also occurred in the Napo Amazon Putumayo and Pacaya Samiria areas (Table 4, Fig. 6). Degradation was the lowest in Ucayali. Relative to palm swamp peatland coverage, the Napo Amazon Putumayo was the area with greatest concentration of degraded palm swamps (13%) while the Marañón - southwest was the area with lowest degradation (5%). Significant deforestation took place in the Ucayali-southeast area (Table 4) and deforestation was the lowest in the Pacaya Samiria reserve. Proportionally to palm swamp peatland extent, Pacaya Samiria had the lowest proportion of deforested palm swamp (0.48%) while Ucayali was the area with the highest proportion (6%).

Changes in degradation and deforestation rates over time varied geographically (Table 5). While Pacaya Samiria and Napo Amazon Putumayo areas experienced reduced degradation rates between 1990-2007 and 2007–2018, elsewhere the degradation rate increased, with the largest increase in Ucayali-southeast. The deforestation rate increased everywhere except for Ucayali and soared in the Marañón-southwest area.

The spatial distribution of degradation and deforestation also changed over time. For instance, within the Pastaza-Marañón degradation shifted from northwest to southeast between 1990-2007 and 2007–2018 (Fig. 6). In the Napo Amazon Putumayo area, degradation along major rivers in 1990–2007 reduced substantially in the most recent period. The expansion of deforestation within the Pastaza-Marañón area mostly occurred along the Marañón River (Figures SI 6-7). In the Ucayali-Southeast, degradation and deforestation were clustered in the north in 1990–2007 and were more dispersed in 2007–2018.

3.2.3. C emissions from degradation and deforestation in palm swamp peatlands

Carbon emissions from biomass and peat over 1990–2018 totaled 39.3 ± 3.5 Tg C (Table 6) and were dominated by emissions from
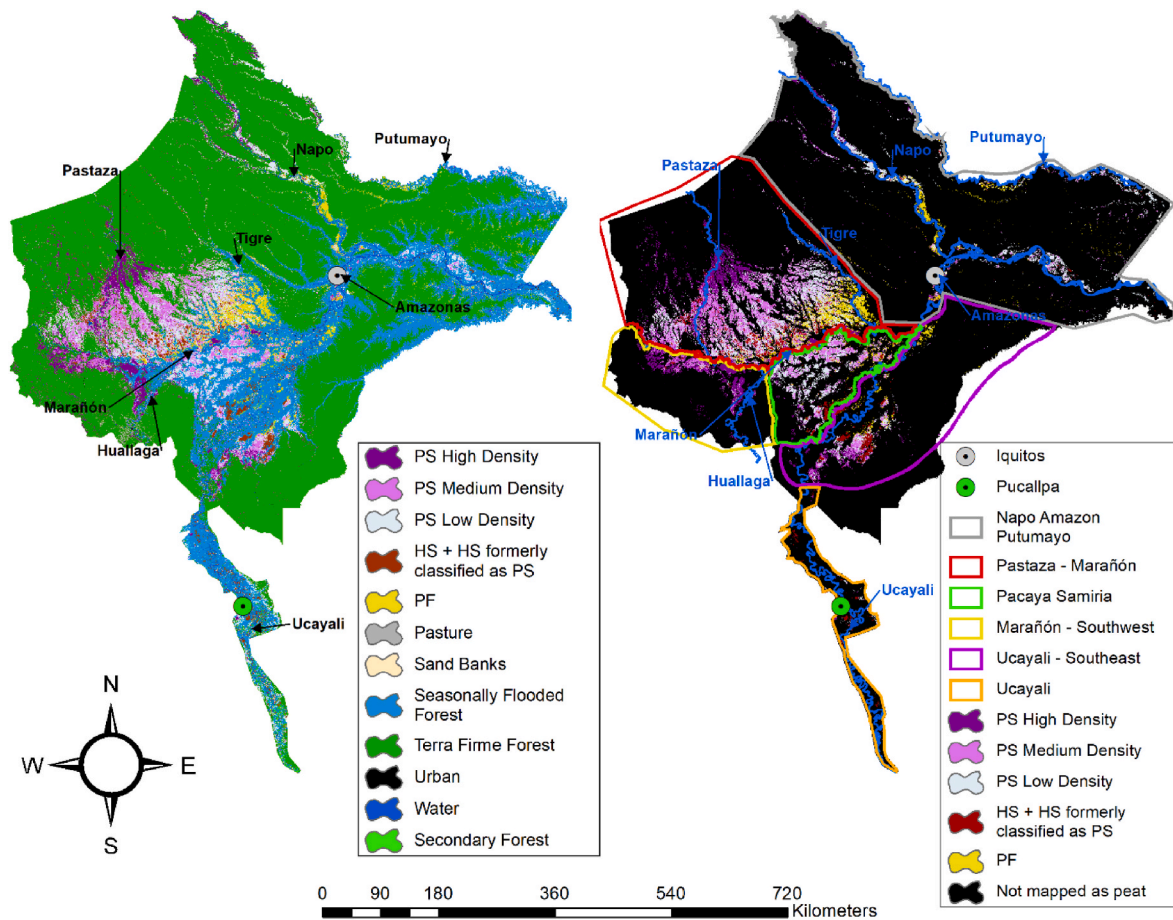
Fig. 3. 2018 land cover map (a) and map of peatlands (b). PS: Palm swamp, HS: Herbaceous swamp, PF: Pole forest. HS classified as PS in former years were included in the HS class. Pixel resolution of maps a and b are 30m.

Table 2
Total area ±SE (ha) of peatlands per geographical area. PS: Palm swamp, HS: Herbaceous swamp, PF: Pole forest.

	Napo Amazon Putumayo	Pastaza - Marañón	Pacaya Samiria	Marañón - southwest	Ucayali - southeast	Ucayali
PS high density	156,947	590,930	42,652	303,987	92,983	12,910
	±6,521	±24,554	±1,772	±12,631	±3,864	±536
PS medium density	69,916	944,549	28,0076	106,263	12,2219	7,718
	±3,108	±41,993	±12,452	±4,724	±5,434	±343
PS low density	315,208	751,592	275,315	12,950	76,115	28,121
	±8,206	±19,568	±7,168	±337	±1,982	±732
HS	20,895	166,565	47,159	8,001	90,702	38,012
	±130	±1,038	±294	±50	±565	±237
PF	111,349	283,832	49,951	158	57,461	0.6
	±2,937	±7,485	±1,317	±4	±1,515	±0.01
All	674,315	2,737,467	695,154	431,359	439,481	86,762
	±11,321	±52,974	±14,539	±13,490	±7,141	±999

degradation (67%). The rate of emissions from degradation increased by 35% in the 2007–2018 period (1.12 ± 0.21 Tg C y^{-1}) as compared to the 1990–2007 period (0.83 ± 0.15 Tg y^{-1}). The emission rate from deforestation increased by 161% from 1990 to 2007 (0.28 ± 0.00 Tg C y^{-1}) to 2007–2018 (0.74 ± 0.01 Tg C y^{-1}). Emissions from degradation and deforestation stemmed largely from the peat (88% and 60%, respectively).

4. Discussion

4.1. Peat-forming ecosystems and C stocks

The extent of peat-forming ecosystems mapped in our study is far larger than the estimates by Draper et al. (2014), and Bourgeau-Chavez et al. (2021), who focused their research on the Pastaza-Marañón basin, and similar to, but still larger than, the appraisal by Hastie et al. (2022) for the whole lowland Peruvian Amazon (6.1 ± 0.3 Mha) (Table SI 9). The large dominance of palm swamps over other peat-forming ecosystems (79%) concurs with findings by Draper et al. (2014), Honorio Coronado et al. (2021) and Hastie et al. (2022). However, our results provided further insights about palm swamps stratified in three levels of palm density, low (2.1 Mha), medium (1.8 Mha) and high (1.6 Mha) (Table 1) which offered us the possibility to refine biomass C stock estimates in this ecosystem.

We found a lower extent of peatlands than Hastie et al. (2022) (5.1 ± 0.1 vs. 6.2 ± 0.2 Mha, Table SI 9) which is driven by the spatial
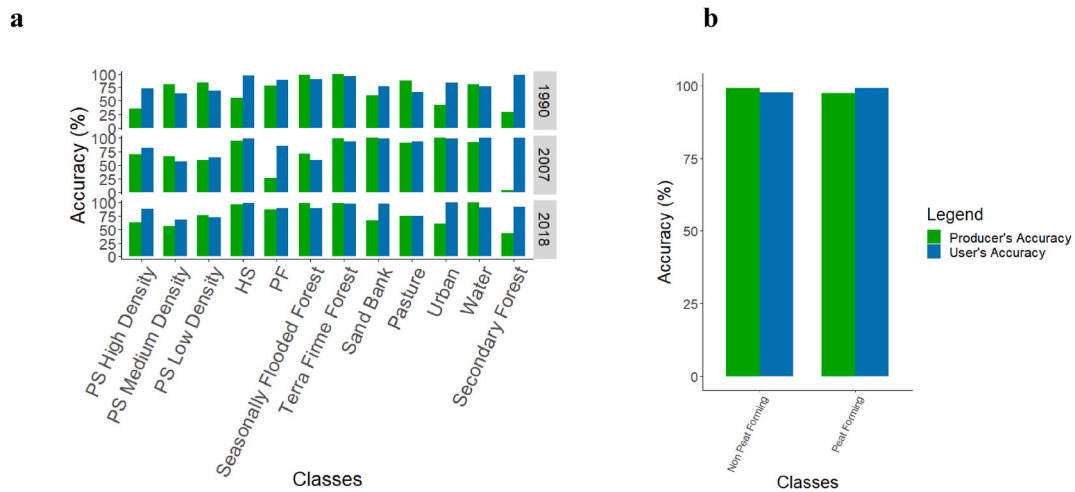
Fig. 4. Accuracy assessments of the classifications for the years 1990, 2007, and 2018 (a), and of all peat-forming and all non-peat forming classes in 2018 (b). PS: Palm swamp, HS: Herbaceous swamp, PF: Pole forest.

Table 3

C stock $\pm$ SE (Pg) in the above-ground biomass (AGB), below-ground biomass (BGB), the soil and in total per peat-forming class in 2018. PS: Palm swamp, HS: Herbaceous swamp, PF: Pole forest.

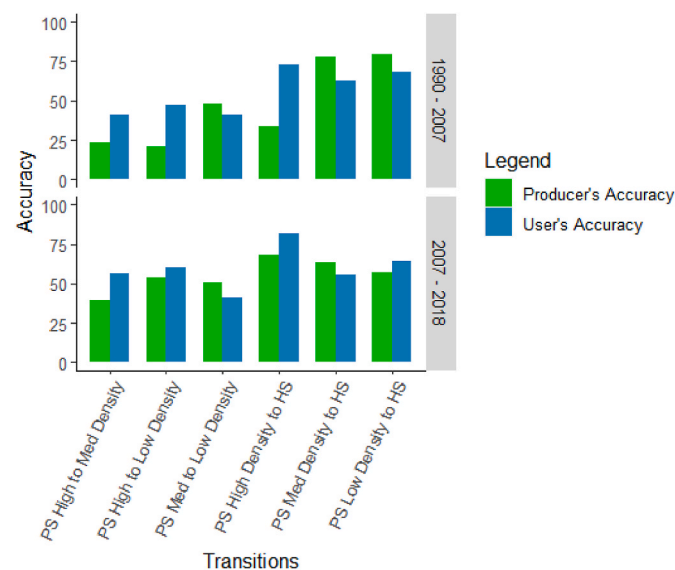| Class	AGB	BGB	Peat	Total
PS high density	0.09 ± 0.006	0.03 ± 0.003	0.78 ± 0.059	0.89 ± 0.06
PS medium density	0.1 ± 0.007	0.03 ± 0.004	1.00 ± 0.077	1.13 ± 0.08
PS low density	0.09 ± 0.006	0.03 ± 0.003	0.94 ± 0.064	1.06 ± 0.06
HS	0 ± n.a.	0.00 ± n.a.	0.22 ± 0.023	0.22 ± 0.02
HS formerly classified as PS	0 ± n.a.	0.00 ± n.a.	0.02 ± 0.008	0.02 ± 0.001
PF	0.04 ± 0.003	0.01 ± 0.001	0.52 ± 0.026	0.57 ± 0.03
All	0.32 ± 0.01	0.10 ± 0.006	3.46 ± 0.12	**3.88 ± 0.12**

Fig. 5. Accuracy of palm swamps transitions for the 1990–2007 period (top) and 2007–2018 period (bottom). PS: Palm swamp, HS: Herbaceous swamp.

distribution of peat-forming ecosystems in the map and assumptions related to peat-forming ecosystems rather than by the smaller area of our study. In contrast to findings by Hastie et al. (2022), our analysis indicated that not all the area of peat-forming ecosystems overlaid peat but only on average 73% did so. This spatial land cover discrepancy resulted in an extent of peat-forming classes over peat 16% lower than the estimate by Hastie et al. (2022). Furthermore, seasonally flooded forest where peat is rare or absent (Honorio Coronado et al., 2021) was not part of the peat-forming ecosystems we considered while Hastie et al. (2022) found 195,100 ha of seasonally flooded forest over peat. These two points highlight that extensive field work is still needed to improve our knowledge on the occurrence of peat in peat-forming ecosystems and in seasonally flooded forests.

In agreement with previous studies, our results demonstrated the prominent role played by palm swamps in storing C in the region, accounting for 79% of the total C stock (Table 3). The peatland C stock in the above-ground biomass and the soil is 72% of the finding by Hastie et al. (2022) (Table SI 10) due to a smaller peatland area but also to a more conservative C density in the biomass of herbaceous swamps (0 here vs. 41 Mg C ha^{-1}). Importantly, the soil average C densities derived from spatially-explicit C stocks by Hastie et al. (2022) were 23% and 41% higher than the default values we used for palm swamp and herbaceous swamp, respectively, which are based on field data (Honorio Coronado et al., 2021).

4.2. Palm swamp peatland degradation and deforestation and associated C emissions

We found a large predominance of degradation over deforestation in palm swamp peatlands. A tendency towards greater degradation than deforestation has also been observed in the Brazilian Amazon (Matricardi et al., 2020), within the whole Amazon basin (Bullock et al., 2020a), and in South American forests (Vancutsem et al., 2021) but not as marked for palm swamps. The 14% increase in the rate of degradation between 2007-2018 and 1990–2007 (Table 5) is in accordance with the rising demand of *M. flexuosa* fruits in the market of Iquitos in the last three decades (Horn et al., 2012, 2018; Endress et al., 2013). Horn et al. (2018) estimated that the annual demand for the fruit in Iquitos in 2012–2013 was 8,206 mT which represents a 49% increase compared to the assessment for 1983–1984 made by Padoch (1988). While efforts have been made to encourage the climbing of palms for collecting their fruits, cutting remains the most common harvesting technique (Romulo et al., 2022).

Degradation was most prominent in the Napo-Amazon-Putumayo,

Table 4

Area ±SE (ha) of degradation and deforestation per geographic area for both time periods and percentage of palm swamp peatlands degraded and deforested in 2018.

	Napo Amazon Putumayo	Pastaza - Marañón	Pacaya Samiria	Marañón - southwest	Ucayali - southeast	Ucayali	All
Degradation 1990–2007	47,844 ±2,001	143,880 ±6,016	45,570 ±1,905	10,931 ±457	11,454 ±479	2,548 ±107	262,227 ± 6,654
Degradation 2007–2018	25,318 ±991	122,832 ± 4,807	18,570 ± 727	11,692 ±458	14,031 ±549	1,734 ± 68	194,177 ± 5,013
Degradation 1990–2018	73,162 ±2,233	266,712 ± 7,701	64,140 ± 2,039	22,623 ±647	25,485 ±729	4,282 ±127	**456,404 ± 8,331**
% Degraded	13	12	11	5	9	9	**11**
Deforestation 1990–2007	1,979 ±51	21,423 ±555	1,439 ±37	672 ±17	5,142 ±133	2,201 ± 57	32,856 ±577
Deforestation 2007–2018	2,881 ±90	33,332 ±1,042	1,422 ±44	2,504 ±78	5,257 ±164	767 ±24	46,163 ±1,063
Deforestation 1990–2018	4,860 ±103	54,755 ±1,181	2,861 ±57	3,176 ±80	10,399 ±211	2,968 ± 62	**79,019 ± 1,209**
% Deforested	1	2	0	1	4	6	**2**

Table 5

Degradation and deforestation rates (ha yr^{-1}) per period and their change across period (%) per geographical area and for the full study area.

		Napo Amazon Putumayo	Pastaza - Marañón	Pacaya Samiria	Marañón - southwest	Ucayali - southeast	Ucayali	All
Degradation	1990–2007	2,814 ±118	8,464 ±354	2,680 ±112	643 ±27	674 ±28	150 ±6	15,424 ±391
	2007–2018	2,302 ±90	11,167 ±437	1,690 ±66	1,063 ±42	1,276 ±50	158 ±6	17,653 ±456
	Percent change	−18	32	−37	65	89	5	**14**
Deforestation	1990–2007	116 ±3	1,260 ±33	85 ±2	40 ±1	303 ±8	129 ±3	1,933 ±34
	2007–2018	262 ±8	3,030 ±95	130 ±4	228 ±7	478 ±15	70 ±2	4,197 ±97
	Percent change	126	140	53	476	58	−46	**117**

Pastaza-Marañón, and Pacaya-Samiria areas during the full study period, with the Pastaza-Marañón accounting for most of the recent period's degradation (Table 4). The region along the Marañón River is known to be the largest source of *M. flexuosa* fruit for the Iquitos market, accounting for more than 50% of the supply in 2012–2013 (Horn et al., 2018). The estimated degradation in the Pacaya-Samiria National Reserve concurs with the studies by Hergoualc'h et al. (2017), Bhomia et al. (2019) and Hidalgo Pizango et al. (2022) who found evidence of degradation in palm swamps with degradation levels varying from moderate to high. Destructive harvest is known to have occurred in the Pacaya-Samiria in the past, likely generating degradation, but this practice significantly declined in the reserve following efforts to promote sustainable harvest methods beginning in 2002 (Hidalgo Pizango et al., 2022). Relative to its palm swamp peatland extent, the Marañón-southwest was the least degraded area potentially due to its lack of connection to the Iquitos market (Horn et al., 2018). However, those swamps are relatively close to the town of Yurimaguas, which may be a market destination for the fruit as well, likely explaining the recent increase in the degradation rate. Future studies on the *M. flexuosa* trade should consider the magnitude of the fruit bound for Yurimaguas, and any other destination, in addition to Iquitos.

The Pastaza-Marañón, Ucayali-southeast and Marañón-southwest areas experienced the most significant increases in degradation rates, which is consistent with the results of Horn et al. (2018). According to these authors, Ucayali is an area that contributed significantly to the Iquitos *M. flexuosa* fruit market in 2012–2013. In addition, the levels of degradation described by Hidalgo Pizango et al. (2022) based on field data on the current proportion of *M. flexuosa* females to males in stands is consistent with our findings. Decreased degradation in the Pacaya-Samiria National Reserve over time may be associated with a shift to climbing palms, which, rather than cutting them down, has been promoted as a sustainable way to harvest *M. flexuosa* fruit since 2002 within the reserve (Baker et al., 2020; Hidalgo Pizango et al., 2022). In some of the highly degraded areas, the spatial pattern of degradation varied considerably between the two studied periods. Within the Napo-Amazon-Putumayo area, far more degradation occurred along the Napo and Amazonas Rivers in 1990–2007 than in 2007–2018, and within the Pastaza-Marañón, degradation shifted from the west in the early period towards the Tigre and Marañón rivers in the east during the later period. These observations agree with publications reporting extensive harvesting of *M. flexuosa* along the Napo during the 1990's (Padoch, 1992) and a marginal fruit production in the Napo region compared to the Pastaza-Marañón in more recent years (Horn et al., 2018). Areas with prominent degradation and rising rates should be targeted for efforts aimed at promoting sustainable management of palm swamps.

The largest percentage of deforested palm swamp peatlands was in the Ucayali area. This is consistent with the very high levels of deforestation nearby Pucallpa (Geobosques, 2021) which are driven by the expansion of commercial agriculture and road construction (Bax et al., 2016; Rojas et al., 2021). However, the rate of deforestation in Ucayali's palm swamp peatlands fell in the recent period, suggesting a potential depletion of the resource due to past overexploitation. The soaring of the deforestation rate in the Marañón-southwest area is also in accordance with high levels of deforestation in neighboring San Martin (Rojas et al., 2021). Less information is available about the drivers of deforestation in the Napo Amazon Putumayo area where we also observed an increase of the deforestation rate in palm swamps. These observations demonstrate the need to investigate more closely the drivers of palm swamp deforestation and to target the aforementioned areas for restoration.

At the scale of the PMFB (considering Pacaya-Samiria, Pastaza-Marañón, Ucayali-southeast and Marañón-southwest), we found a deforestation rate of 3,866 ha y^{-1} over 2007–2018, which is far greater than the estimates by Bourgeau-Chavez et al. (2021) for all peat-forming ecosystems (284 ha y^{-1}) and for only palm swamps (44 ha y^{-1}). According to this study which was based on the MINAM Geobosques product, 1,920 ha of pole forests and only 349 ha of palm swamps were lost due to deforestation from 2010 to 2018 across the PMFB. A similar dataset by MINAM Geobosques was used by Hastie et al. (2022) who estimated 5,056 ha y^{-1} of deforestation in the Peruvian Amazon
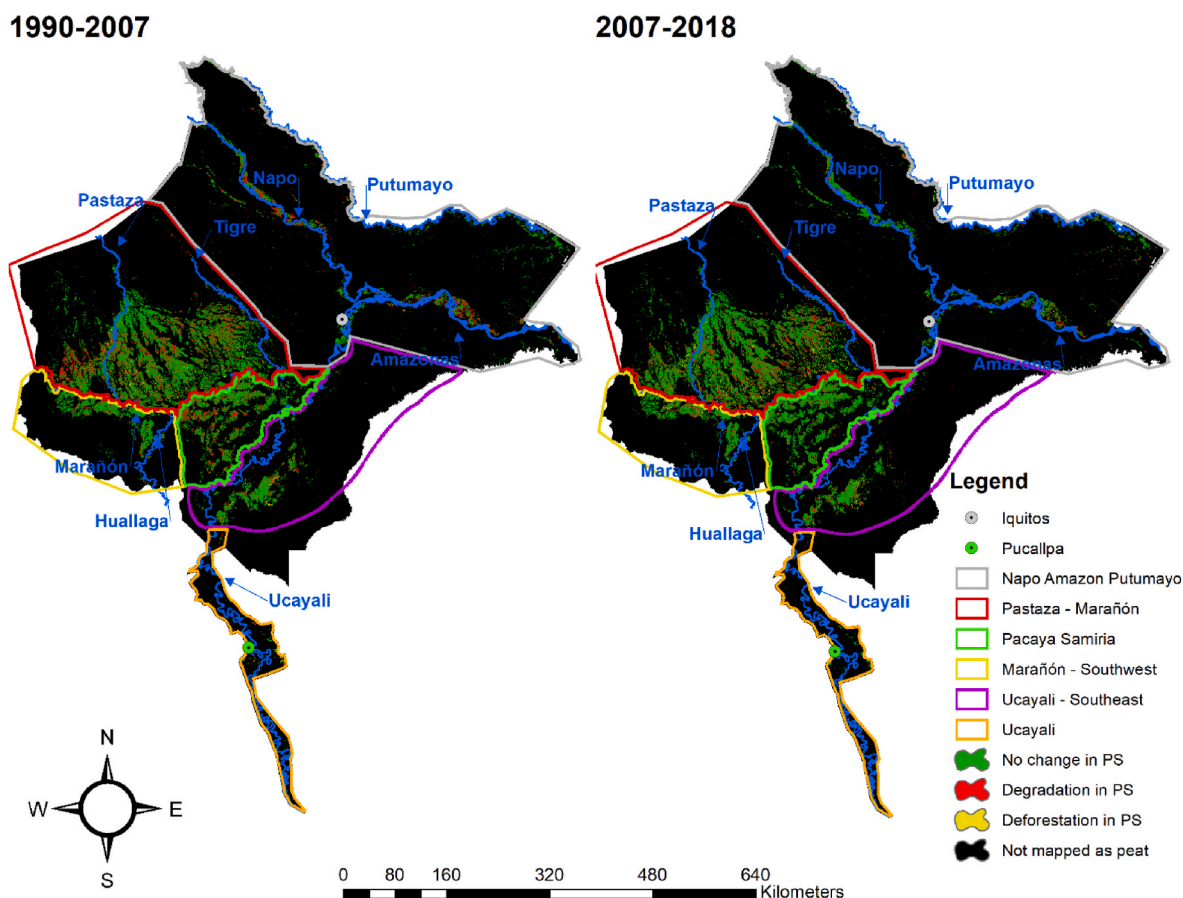
1990-2007   2007-2018

Fig. 6. Spatial distribution of palm swamp degradation and deforestation on peat for the periods 1990–2007 and 2007–2018. Green indicates no change in palm swamps over time. Red displays degradation in palm swamps i.e., a drop in palm density. Yellow depicts palm swamp deforestation i.e., palm swamp to herbaceous swamp transition. PS: Palm swamp.

Table 6
Carbon emissions $\pm$ SE (Tg) resulting from degradation and deforestation of palm swamp peatlands during the periods 1990–2007, 2007–2018 and over both periods.

	1990–2007			2007–2018			1990–2018		
Activity	AGB	Peat	Total	AGB	Peat	Total	AGB	Peat	Total
Degradation	1.7	12.3	14.1	1.3	11.0	12.3	3.1	23.3	26.3
	±1.0	±2.4	±2.6	±0.7	±2.2	±2.4	±1.2	±3.3	±3.5
Deforestation	2.1	2.7	4.8	3.0	5.2	8.1	5.1	7.8	12.9
	±0.1	±0.2	±0.3	±0.1	±0.5	±0.5	±0.2	±0.5	±0.5
Degradation and deforestation	3.9	15.0	18.9	4.3	16.1	20.4	8.2	31.1	39.3
	±1.0	±2.4	±2.6	±0.7	±2.3	±2.4	±1.2	±3.3	±3.5

peatlands for the period 2000–2016, a value comparable to our result over 2007–2018 (4,163 ± 1,063 ha y^{-1} of palm swamp peatlands deforested, Table 4). However, most deforestation identified by Hastie et al. (2022) was concentrated near Pucallpa in the Ucayali department while we found that 72% of the deforested palm swamps were in the Loreto department, specifically in the Pastaza-Marañón area. The Geobosques product used a spectral mixture analysis to identify forest and non-forest with deforested areas distinguished based on spectral changes associated with the presence of bare soil or downed trees. In contrast, our deforestation detection method based on a categorical transition from palm swamp to herbaceous swamp does not necessarily involve a strong spectral response associated with the exposure of dead wood and soil. While both methods are well founded, they require validation of results using ground truthing data.

With regards to carbon emissions, the peat emission rate from palm swamp deforestation over 2007–2018 (0.46 Tg C y^{-1}) is almost twice the rate found by Hastie et al. (2022) (0.27 Tg C y^{-1}). This difference is due

to dominant transition types (low density palm swamp to herbaceous swamp in our study versus forest to agriculture and secondary vegetation in their analysis) and associated peat emission factors. Notably, Hastie et al. (2022) used IPCC defaults which are based on data from Southeast Asian peatlands whereas we considered palm swamp-specific emission factors measured in Peru (Table SI 7). The annual AGB emission rate from deforestation in 2007–2018 (0.27 Tg C y^{-1}) is lower than the rate reported in the national Forest Reference Emission Level (MINAM., 2021) 2021 for deforestation-AGB loss in the entire hydromorphic zone in 2010–2019 (0.47 Tg C y^{-1}). Given that the hydromorphic zone encompasses all flooded forest types (seasonally flooded forests, pole forests and palm swamps), a lower estimate for solely palm swamp peatlands seems reasonable. While the FREL 2021 (MINAM., 2021) only considers deforestation emissions in the AGB pool, we roughly estimate that including palm swamp degradation in addition to deforestation and the soil as another pool would increase national forest emissions by 75% and 6%, in the hydromorphic zone and in the whole

Peruvian Amazon, respectively. For this assessment, we assumed that: 1) half of deforestation-AGB emissions in the hydromorphic zone is in palm swamp peatlands, and as found for 2007–2018 2) the deforestation peat: AGB emission ratio equals 1.7, and 3) the degradation: deforestation emission ratio is 1.1. These estimations which only consider palm swamp peatlands regardless of degradation in other peat-forming ecosystems highlight the importance of including peatland emissions in national C accounting.

4.3. Detecting palm swamp degradation with remote sensing

Neither the Peruvian national REDD + program nor its NDCs account yet for emissions from forest degradation. A method that has been proposed for detecting degradation at the national level is based on the assumption that degradation borders deforestation and consists of analyzing morphological spatial patterns of deforestation as a proxy measure for degradation (Argotty et al., 2019). Our results suggest that such a method would not be suitable for detecting degradation in palm swamp peatlands which is not necessarily contiguous to deforested areas. Instead, our method of analyzing transitions is useful in detecting selective logging and other land cover changes that are typically difficult to detect directly with remote sensing (Peres et al., 2006), which is critically important given the high C losses of perturbed peatlands. Our methods present a methodological challenge however, as inaccuracies between classifications compound when calculating a transition. Lower transition accuracy may result in an overestimation of degradation. Due to the large size and very limited accessibility of the study area, training and validation data were not randomly collected (Olofsson et al., 2014) and were limited to places where high-resolution images existed or were successfully captured. We also prioritized heterogeneous land cover areas for high-resolution imagery to optimize training polygons from multiple classes from the same image. The implications on map accuracy and area estimates of such non-random sampling remain to be addressed.

In terms of precision, our producer's and user's accuracies for the degradation transitions (56.4–68.5% user's, 39.5–79.6% producer's; Fig. 5) were within the range obtained by Shimabukuro et al. (2019) (68 and 70% respectively) and Bullock et al. (2020a) (44% and 73%, respectively) suggesting that our method is comparable to other studies assessing forest degradation in the region. Because degradation due to selective logging often results in fast regrowth, a time series approach using spectral mixture analysis has been proposed to detect this form of degradation (Bullock et al., 2020b). Based on the assumption that degraded forests will exhibit a greater proportion of woody vegetation compared to green vegetation, Bullock et al. (2020a) found important forest degradation near deforestation hotspots, such as nearby Pucallpa in Peru, and throughout the "arc of deforestation" in the southern Brazilian Amazon. Nevertheless, their levels of degradation within the Peruvian palm swamps were very low compared to our results. The inclusion of PALSAR and GEDI data in our analysis offers a high detection probability and capacity in capturing palm swamp canopy changes compared to spectral analysis from Landsat data alone, as used by Bullock et al. (2020a). Particularly, PALSAR data can improve the detection of structural changes in forest canopy that do not necessarily translate into sharp spectral characteristics changes.

We determined palm swamp density by visual interpretation of high-resolution images however we recommend future studies to refine land cover calibration and validation based on field data. Estimating palm density in swamps can also be performed using unmanned aerial vehicles, as demonstrated by Tagle Casapia et al. (2020) and Wagner et al. (2020). Integrating these types of images with satellite remote sensing may improve palm density assessments. Furthermore, the 2022 launch of the European Space Agency's BIOMASS sensor, a P-band radar satellite (Gao et al., 2020) and NASA's NISAR L-band radar satellite (NISAR., 2022) could also help to improve the classification accuracy of palm swamp density.

5. Conclusions

Using a remote sensing approach, this study provides the first quantification of deforestation and degradation in palm swamps, the most extensive and threatened peatland ecosystem in the Peruvian Amazon. Our results reveal that deforestation appeared to be limited compared to degradation but that the rate of both activities is accelerating. Resulting C emissions from degradation were higher than those from deforestation and for context, the 39.3 Tg C emissions from both activities over 1990–2018 is approximately 77% of the C emissions emitted in Peru in 2021, from burning fossil fuels and industry. The magnitude of these emissions calls for the country to account for deforestation and degradation of forested peatlands in national C emission reports. Our study provides critical information on where palm swamp conservation and restoration efforts for the region should be focused. The Pastaza-Marañón and Marañón-southwest zones are experiencing fast increases in both degradation and deforestation, and should therefore be targeted for conservation and restoration efforts. In addition, conservation efforts appear to be warranted in the Ucayalisoutheast zone and the Napo Amazon Putumayo. Sustainable techniques to harvest the fruits of *M. flexuosa,* such as climbing, or cutting the racemes with a long-handle saw (Rabelo and França, 2015), should be promoted widely in the region and particularly within areas experiencing surges in palm swamp degradation.

Declaration of competing interest

The authors declare that they have no known competing financial interests or personal relationships that could have appeared to influence the work reported in this paper.

Data availability

Data will be made available on request.

Appendix A. Supplementary data

Supplementary data to this article can be found online at https://doi.org/10.1016/j.jenvman.2023.119665.

References

Argotty, F., Badaracco, R., Campos, L., Mendoza, R., Pino, I., 2019. Estimacion de degradación forestal en el bioma amazonico a partir del enfoque indirecto. MINAM.

Baker, T., Del Castillo Torres, D., Honorio Coronado, E., Lawson, I., Martín Brañas, M., Montoya, M., Roucoux, K., 2020. The challenges for achieving conservation and sustainable development within the wetlands of the Pastaza - Marañon basin, Peru. In: Tirado, Chirif, Alberto (Eds.), Peru: Deforestation in Times of Climate Change, vol. 2019. IWGIA, Lima, pp. 155–174.

Bax, V., Francesconi, W., Quintero, M., 2016. Spatial modeling of deforestation processes in the Central Peruvian Amazon. J. Nat. Conserv. 29, 79–88. https://doi.org/10.1016/j.jnc.2015.12.002.

Bhomia, R.K., van Lent, J., Gradez Rios, J.M., Hergoualc'h, K., Honorio Coronado, E.N., Murdiyarso, D., 2019. Impacts of Mauritia flexuosa degradation on the carbon stocks of freshwater peatlands in the Pastaza Marañon river basin of the Peruvian Amazon. Mitig. Adapt. Strategies Glob. Change 24, 645–668. https://doi.org/10.1007/s11027-018-9809-9.

Bourgeau-Chavez, L.L., Grelik, S.L., Battaglia, M.J., Leisman, D.J., Chimner, R., Hribljan, J.A., Lilleskov, E.A., Draper, F.C., Zutta, B.R., Hergoualc'h, K., Bhomia, R., Lahteenoja, O., 2021. Advances in Amazonian peatland discrimination with multi-temporal PALSAR refines estimates of peatland distribution, C stocks and deforestation. Front. Earth Sci. 9 https://doi.org/10.3389/feart.2021.676748.

Bullock, E.L., Woodcock, C.E., Souza Jr., C., Olofsson, P., 2020a. Satellite-based estimates reveal widespread forest degradation in the Amazon. Global Change Biol. 26, 2956–2969. https://doi.org/10.1111/gcb.15029.

Bullock, E.L., Woodcock, C.E., Olofsson, P., 2020b. Monitoring tropical forest degradation using spectral unmixing and Landsat time series analysis. Remote Sens. Environ. 238, 110968 https://doi.org/10.1016/j.rse.2018.11.011.

Cole, L.E.S., Åkesson, C.M., Hapsari, K.A., Hawthorne, D., Roucoux, K.H., Girkin, N.T., Cooper, H.V., Ledger, M.J., O'Reilly, P., Thornton, S.A., 2022. Tropical peatlands in the anthropocene: lessons from the past. Anthropocene 37. https://doi.org/10.1016/j.ancene.2022.100324.

Dezzeo, N., Grandez-Rios, J., Martius, C., Hergoualc'h, K., 2021. Degradation-driven changes in fine root carbon stocks, productivity, mortality, and decomposition rates in a palm swamp peat forest of the Peruvian Amazon. Carbon Bal. Manag. https://doi.org/10.1186/s13021-021-00197-0.

Draper, F.C., Roucoux, K.H., Lawson, I.T., Mitchard, E.T.A., Honorio Coronado, E.N., Lahteenoja, O., Torres Montenegro, L., Valerrama Sandoval, E., Zarate, R., Baker, T. R., 2014. The distribution and amount of carbon in the largest peatland complex in Amazonia. Environ. Res. Lett. https://doi.org/10.1088/1748-9326/9/12/124017.

Draper, F.C., Honorio Coronado, E.N., Roucoux, K.H., Lawson, I.T., Pitman, N.C.A., Fine, P.V.A., Phillips, O.L., Torres Montenegro, L.A., Valderrama Sandoval, E., Mesones, I., Garcia-Villacorta, R., Ramirez Arevelo, F.R., Baker, T.R., 2018. Peatland forests are the least diverse tree communities documented in Amazonia, but contribute to high regional beta diversity. Ecography 41, 1256–1269. https://doi.org/10.1111/ecog.03126.

Drösler, M, Verchot, LV, Freibauer, A, Pan, G, Evans, CD, Bourbonniere, RA, et al., 2014. Drained inland organic soils. In: Hiraishi, T, Krug, T, Tanabe, K, Srivastava, N, Jamsranjav, B, Fukuda, M, et al. (Eds.), Supplement to the 2006 Guidelines for National Greenhouse Gas Inventories: Wetlands. Intergovernmental Panel on Climate Change, Switzerland.

Endress, B.A., Horn, C.M., Gilmore, M.P., 2013. Mauritia flexuosa palm swamps: composition, Structure and implications for conservation and management. For. Ecol. Manag. 302, 346–353. https://doi.org/10.1016/j.foreco.2013.03.051.

Falen Horna, L.Y., Honorio Coronado, E.N., 2018. Evaluación de las técnicas de aprovechamiento de frutos de aguaje (Mauritia flexuosa Lf) en el distrito de Jenaro Herrera, Loreto, Perú. Folia Amaz. 27 (2), 131–150. https://doi.org/10.24841/fa.v27i2.443.

Fine, P.V.A., Garcia-Villacorta, R., Pitman, N.C.A., Mesones, I., Kembel, S.W., 2010. A floristic study of the white-sand forests of Peru. Ann. Mo. Bot. Gard. 97 (3), 283–305. https://doi.org/10.3417/2008068.

Flores Llampazo, G., Honorio Coronado, E.N., del Aguila-Pasquel, J., Cordova Oroche, C. J., Díaz Narvaez, A., Reyna Huaymacari, J., Grandez Ríos, J., Lawson, I.T., Hastie, A., Baird, A.J., Baker, T.R., 2022. The presence of peat and variation in tree species composition are under different hydrological controls in Amazon wetland forests. Hydrol. Process. 36 (9), e14690 https://doi.org/10.1002/hyp.14690.

Freitas Alvarado, L., Pinedo Panduro, M., Linares Bensimon, C., Del Castillo Torres, D., 2006. In: Descriptores para el aguaje. Instituto de Investigaciones de la Amazon Peruana. https://repositorio.iiap.gob.pe/handle/20.500.12921/229.

Gao, Y., Skutsch, M., Paneque-Galvez, J., Ghilardi, A., 2020. Remote sensing of forest degradation: a review. Environmental Resource Letters 15. https://doi.org/10.1088/1748-9326/abaad7.

Geobosques, 2021. Bosque y no bosque 1000 – perdida de bosque 2001-2000. (Ministerio del Ambiente). https://geobosques.minam.gob.pe/geobosque/view/descargas.php?122345gxxe345w34gg.

Gilmore, M.P., Endress, B.A., Horn, C.M., 2013. The socio-cultural importance of Mauritia flexuosa palm swamps (aguajales) and implications for multi-use management in two Maijuna communities of the Peruvian Amazon. J. Ethnobiol. Ethnomed 9, 1–23.

Glinskis, E., Gutierrez-Velez, V.H., 2019. Quantifying and understanding carbon emissions from land cover changes between large and small oil palm expansion regimes in the Peruvian Amazon. Land Use Pol. 80, 95–106. https://doi.org/10.1016/j.landusepol.2018.09.032.

Gumbricht, T., Roman-Cuesta, R.M., Verchot, L., Herold, M., Wittmann, F., Householder, E., Herold, N., Murdiyarso, D., 2017. An expert system model for mapping tropical wetlands and peatlands reveals South America as the largest contributor. Global Change Biol. 23, 3581–3599. https://doi.org/10.1111/gcb.13689.

Hastie, A., Honorio Coronado, E.N., Reyna, J., Mitchard, E.T.A., Akesson, C.M., Baker, T. R., Cole, L.E.S., Cordova Oroche, C.J., Dargie, G., Davila, N., De Grandi, E.C., Del Aguila, J., del Castillo Torres, D., De La Cruz Paiva, R., Draper, F.C., Flores, G., Grandez, J., Hergoualc'h, K., Householder, J.E., Janovec, J.P., Lahteenoja, O., Reyna, D., Rodriguez-Veiga, Pedro, Roucoux, K.H., Tobler, M., Wheeler, C.E., Williams, M., Lawson, I.T., 2022. Risks to carbon storage from land-use change revealed by peat thickness maps of Peru. Nat. Geosci. https://doi.org/10.1038/s41561-022-00923-4.

Hergoualc'h, K., Verchot, L.V., 2011. Stocks and fluxes of carbon associated with land-use change in Southeast Asian tropical peatlands: a review. Global Biochem. Cycles 25. GB2001.

Hergoualc'h, K., Gutierrez-Velez, V.H., Menton, M., Verchot, L.V., 2017. Characterizing degradation of palm swamp peatlands from space and on the ground: an exploratory study in the Peruvian Amazon. For. Ecol. Manag. 393, 63–73. https://doi.org/10.1016/j.foreco.2017.03.016.

Hergoualc'h, K., Dezzeo, N., Verchot, L.V., Martius, C., van Lent, J., del Aguila-Pasquel, J., Lopez, M., 2020. Spatial and temporal variability of soil N2O and CH4 fluxes along a degradation gradient in a palm swamp peat forest in the Peruvian Amazon. Global Change Biol 26 (12), 7198–7216. https://doi.org/10.1111/gcb.15354.

Hergoualc'h, K., van Lent, J., Dezzeo, N., Verchot, L.V., van Groenigen, J.W., Lopez, M., Grandez-Rios, J., 2023. Major CO_2 losses from degradation of Mauritia flexuosa peat swamp forests in western Amazon. Biogeochemistry. https://doi.org/10.1007/s10533-023-01057-4.

Hidalgo Pizango, C.G., Honorio Coronado, E.N., del Águila-Pasquel, J., et al., 2022. Sustainable palm fruit harvesting as a pathway to conserve Amazon peatland forests. Nat. Sustain. 5, 479–487. https://doi.org/10.1038/s41893-022-00858-z.

Holm, J.A., Miller, C.J., Cropper, W.P., 2008. Population dynamics of the dioecious Amazonian palm Mauritia flexuosa: simulation analysis of sustainable harvesting. Biotropica 40, 550–558. https://doi.org/10.1111/J.1744-7429.2008.00412.

Honorio Coronado, E.N., Hastie, A., Reyna, J., Flores, G., Grández, J., Lähteenoja, O., Draper, F.C., Åkesson, C.M., Baker, T.R., Bhomia, R.K., Cole, L.E.S., Dávila, N., del Águila, J., del Águila, M., del Castillo Torres, D., Lawson, I.T., Martín Brañas, M., Mitchard, E.T.A., Monteagudo, A., Phillips, O.L., Ramírez, E., Ríos, M., Ríos, S., Rodriguez, L., Roucoux, K.H., Tagle Casapia, X., Vasquez, R., Wheeler, C.E., Montoya, M., 2021. Intensive field sampling increases the known extent of carbon-rich Amazonian peatland pole forests. Environ. Res. Lett. 16 (7), 074048.

Horn, C.M., Gilmore, M.P., Endress, B.A., 2012. Ecological and socio-economic factors influencing aguaje (*Mauritia flexuosa*) resource management in two indigenous communities in the Peruvian Amazon. For. Ecol. Manag. 267, 93–103. https://doi.org/10.1016/j.foreco.2011.11.040.

Horn, C.M., Vargas Paredes, V.H., Gilmore, M.P., Endress, B.A., 2018. Spatio-temporal patterns of Mauritia flexuosa fruit extraction in the Peruvian Amazon: implications for conservation and sustainability. Appl. Geogr. 97, 98–108. https://doi.org/10.1016/j.apgeog.2018.05.004.

Householder, J.E., Janovec, J.P., Tobler, M.W., Page, S., Lähteenoja, O., 2012. Peatlands of the Madre de Dios river of Peru: distribution, geomorphology, and habitat diversity. Wetlands 32, 359–368. https://doi.org/10.1007/s13157-012-0271-2.

Kalliola, R., Puhakka, M., Salo, J., Tuomisto, H., Ruokolainen, K., 1991. The dynamics, distribution and classification of swamp vegetation in the Peruvian Amazon. Ann. Bot. Fenn. 28, 225–239.

Kelly, T.J., Lawson, I.T., Roucoux, K.H., Baker, T.R., Jones, T.D., Sanderson, N.K., 2017. The vegetation history of an Amazonian domed peatland. Palaeogeogr. Palaeoclimatol. Palaeoecol. 468, 129–141. https://doi.org/10.1016/j.palaeo.2016.11.039.

Kelly, T.J., Lawson, I.T., Roucoux, K.H., Baker, T.R., Honorio Coronado, E.N., 2020. Patterns and drivers of development in a west Amazonian peatland during the late Holocene. Quaternary Science Reviews. 230. https://doi.org/10.1016/j.quascirev.2020.106168.

Lähteenoja, O., Ruokolainen, K., Schulman, L., Alvarez, J., 2009a. Amazonian floodplains harbour minerotrophic and ombrotrophic peatlands. Catena 79, 140–145. https://doi.org/10.1016/j.catena.2009.06.006.

Lähteenoja, O., Ruokolainen, K., Schulman, L., Oinonen, M., 2009b. Amazonian peatlands: an ignored C sink and potential source. Global Change Biol. 15, 2311–2320. https://doi.org/10.1016/j.palaeo.2016.11.039.

Lähteenoja, O., Page, S., 2011. High diversity of tropical peatland ecosystem types in the Pastaza-Marañón basin, Peruvian Amazonia. J. Geophys. Res.Biogeosci. 116 (G2) https://doi.org/10.1029/2010JG001508.

Lähteenoja, O., Reátegui, Y.R., Räsänen, M., Del Castillo Torres, D., Oinonen, M., Page, S., 2012. The large Amazonian peatland carbon sink in the subsiding Pastaza-Marañón foreland basin, Peru. Global Change Biol. 18, 164–178. https://doi.org/10.1111/j.1365-2486.2011.02504.x.

Lawson, I.T., Honorio Coronado, E.N., Andueza, L., Cole, L., Dargie, G.C., Davies, A.L., Laurie, N., Okafor-Yarwood, I., Roucoux, K.H., Simpson, M., 2022. The vulnerability of tropical peatlands to oil and gas exploration and extraction. Progress in Environmental Geography. https://doi.org/10.1177/27539687221124046.

Limpens, J., et al., 2008. Peatlands and the carbon cycle: from local processes to global implications – a synthesis. Biogeosciences 5, 1475–1491. https://doi.org/10.5194/bg-5-1475-2008.

Lo, E., 2005. Gaussian error propagation applied to ecological data: post-ice-storm-downed Woody biomass. Ecol. Monogr. 75 (4), 451–466. https://doi.org/10.1890/05-0030.

López Gonzales, M., Hergoualc'h, K., Angulo Núñez, Ó., et al., 2020. What do we know about Peruvian peatlands? Occasional Paper 210 CIFOR, Bogor, Indonesia. https://doi.org/10.17528/cifor/007848.

Malhi, Y., Aragao, L.E.O.C., Metcalfe, D.B., Paiva, R., Quesadas, C.A., Almeida, S., Anderson, L., Brando, P., Chambers, J.Q., Da Costa, A.C.L., Hutyra, L.R., Oliveria, P., Patiño, S., Pyle, E.H., Roberson, A.L., Teixeria, L.M., 2009. Comprehensive assessment of carbon productivity, allocation and storage in three Amazon forests. Global Change Biology.15 1255–1274. https://doi.org/10.1111/j.1365-2486.2008.01780.x.

Matricardi, E.A.T., Skole, D.L., Costa, O.B., Pedlowski, M.A., Samek, J.H., Miguel, E.P., 2020. Long-term forest degradation surpasses deforestation in the Brazilian Amazon. Science 369 (6509), 1378–1382. https://doi.org/10.1126/science.abb3021.

MINAM, 2015. Mapa de cobertura vegetal. https://geoservidor.minam.gob.pe/wp-content/uploads/2017/06/Mapa_ecosistemas_2018.pdf.

MINAM, 2021. Nivel de referencia de emisiones forestales por deforestación bruta del Peru en el bioma Amazonica.

Murdiyarso, D., Lilleskov, E., Kolka, R., 2019. Tropical peatlands under siege: the need for evidence-based policies and strategies. Mitig. Adapt. Strategies Glob. Change 24, 493–505. https://doi.org/10.1007/s11027-019-9844-1.

NISAR, 2022. NISAR NASA ISRO SAR Mission. https://nisar.jpl.nasa.gov/.

Olofsson, P., Foody, G.M., Herold, M., Stehman, S.V., Woodcock, C.E., Wulder, M.A., 2014. Good practices for estimating area and assessing accuracy of land change. Rem. Sens. Environ. 148, 42–57. https://doi.org/10.1016/j.rse.2014.02.015.

Padoch, C., 1988. Aguaje (Mauritia flexuosa L.f.) in the economy of Iquitos, Peru. Adv. Econ. Bot. 6, 214–224.

Padoch, C., 1992. Marketing of non-timber forest products in Western Amazon: general observations and research priorities. Adv. Econ. Bot. 9, 43–50.

Palacios, J., Zarate, R., Torres, G., Denux, J.-P., Maco, J., Gallardo, G., Mori, T., Rengifo, J., Jarama, A., Marin, M., Garcia, F., Cuadros, A., 2016. Mapeo de los bosques tipo varillal utilizando imágenes de satélite Rapideye en la provincia Maynas, Loreto, Peru. Instituto de Investigaciones de la Amazon Peruana. 25, 25–36.

Penn, J., 2008. Non-timber forest products in Peruvian Amazon: changing patterns of economic exploitation. Focus Geogr. 51 (No. 2).

Peres, C.A., Barlow, J., Laurance, W.F., 2006. Detecting anthropogenic disturbance in tropical forests. Trends Ecol. Evol. 21 (5), 227–229. https://doi.org/10.1016/j.tree.2006.03.007.

Petrescu, A.M.R., et al., 2015. The uncertain climate footprint of wetlands under human pressure. Proc. Natl. Acad. Sci. USA 112 (15), 4594–4599.

Potapov, P.V., Hansen, M., Kommareddy, I., Kommareddy, A., Turubanova, S., Pickens, A., Adusei, B., Tyukavina, A., Ying, Q., 2020. Landsat analysis ready data for global land cover and land cover change mapping. Rem. Sens. 2020 (12), 426. https://doi.org/10.3390/rs12030426(Potapov_RS_2020.pdf).

Rabelo, A., França, F., 2015. Buriti: coleta, pós-colheita, processamento e beneficiamento dos frutos de buriti (Mauritia flexuosa L. f.). Instituto Nacional de Pesquisas da Amazônia.

Revilla-Chavez, J., Lluncor Montalvan, J.M., Garcia Soria, D., Rojas Mego, D.G., Abanto Rodriguez, K., Guerra Arevalo, C., Mejia Carhuanca, W.F., Del Castillo, K., Torres, D., 2019. Distribucion espacial de aguajales mediante clasificacion supervisada de imagenes de sateelite de la region Ucayali, Peru. Folia Amaz. 28 (2), 161–175.

Rojas, E., Zutta, B.R., Velazco, Y.K., Montoya-Zumaeta, J.G., Salva-Catarineu, M., 2021. Deforestation risk in the Peruvian Amazon basin. Environ. Conserv. 48 (4) https://doi.org/10.1017/S0376892921000291.

Romulo, C., Kennedy, C.J., Gilmore, M.P., Endress, B.A., 2022. Sustainable harvest training in a common pool resource setting in the Peruvian Amazon: limitations and opportunities. Trees, Forests and People. https://doi.org/10.1016/j.tfp.2021.100185.

Roucoux, K.H., Lawson, I.T., Jones, T.D., Baker, T.R., Honorio Coronado, E.N., Gosling, W.D., Lahteenoja, O., 2013. Vegetation development in an Amazonian peatland. Palaeogeogr. Palaeoclimatol. Palaeoecol. 374, 242–255. https://doi.org/10.1016/j.palaeo.2013.01.023.

Roucoux, K.H., Lawson, I.T., Baker, T.R., del Castillo Torres, D., Draper, F.C., Lähteenoja, O., Gilmore, M.P., Honorio Coronado, E.N., Kelly, T.J., Mitchard, E.T.A., Vriesendorp, C.F., 2017. Threats to intact tropical peatlands and opportunities for their conservation. Conserv. Biol. 31, 1283–1292. https://doi.org/10.1111/cobi.12925.

Schultz, C., Branas, M.M., Nunez-Perez, C., Del Aguila Villacorta, M., Laurie, N., Lawson, I.T., Roucoux, K.H., 2019. Uses, cultural significance, and management of

peatlands in the Peruvian Amazon: implications for conservation. Biol. Conserv. 235, 189198. https://doi.org/10.1016/j.biocon.2019.04.005.

Shimabukuro, Y., Arai, E., Duarte, V., Jorge, A., Ghizoni dos Santos, E., Cruz Gasparini, K.A., Cerqueira Dutra, A., 2019. Monitoring deforestation and forest degradation using multi-temporal fraction images derived from Landsat sensor data in the Brazilian Amazon. Int. J. Rem. Sens. 40 (14), 5475–5496. https://doi.org/10.1080/01431161.2019.1579943 [CrossRef Partial][Check "vol" partially styled, Check multiple atl].

Stehman, S.V., Foody, G.M., 2019. Key issues in rigorous accuracy assessment of land cover products. Rem. Sens. Environ. 231 https://doi.org/10.1016/j.rse.2019.05.018.

Swails, E., Hergoualc`h, K., Verchot, L., Novita, N., Lawrence, D., 2021. Spatio-Temporal variability of peat CH$_4$ and N$_2$O fluxes and their contribution to peat GHG budgets in Indonesian forests and oil palm plantations. Front. Environ. Sci. 9, 1–15. https://doi.org/10.3389/fenvs.2021.617828.

Swindles, G.T., Morris, P.J., Whitney, B., Galloway, J.M., Galka, M., Gallego-Sala, A., Macumber, A.L., Mullan, D., Smith, M.W., Amesbury, M.J., Roland, T.P., Sanei, H., Patterson, R.T., Sanderson, N., Parry, L., Charman, D.J., Lopez, O., Valderamma, E., Watson, E.J., Ivanovic, R.F., Valdes, P.J., Turner, T.E., Lahteenoja, O., 2017. Ecosystem state shifts during long-term development of an Amazonian peatland. Global Change Biol. https://doi.org/10.1111/gcb.13950.

Tagle Casapia, X., Falen, L., Bartholomeus, H., Cardenas, R., Flores, G., Herold, M., Honorio Coronado, E.N., Baker, T.R., 2020. Identifying and quantifying the abundance of economically important palms in the tropical moist forest using UAV imagery. Rem. Sens. 12 (1), 9. https://doi.org/10.3390/rs12010009.

van der Hoek, Y., Alvarez Solas, S., Penuela, M.C., 2019. The palm Mauritia flexuosa, a keystone plant resource on multiple fronts. Biodivers. Conserv. 28 (3), 539–551. https://doi.org/10.1007/s10531-018-01686-4.

van Lent, J., Hergoualc'h, K., Verchot, L., Oenema, O., willem van Groenigen, J., 2019. Greenhouse gas emissions along a peat swamp forest degradation gradient in the Peruvian Amazon: soil moisture and palm roots effects. Mitig. Adapt. Strategies Glob. Change 24, 625–643. https://doi.org/10.1007/s11027-018-9796-x.

Vancutsem, C., Achard, F., Vielledent, G., Carboni, S., Simonetti, D., Gallego, J., Aragao, L.E.O.C., Nasi, R., 2021. Long-term (1990-2019) monitoring of forest cover changes in the humid tropics. Sci. Adv. 7 (10).

Virapongse, A., Endress, B.A., Gilmore, M.P., Horn, C., Romulo, C., 2017. Ecology, livelihoods, and management of the *Mauritia flexuosa* palm in South America. Global Ecology and Conservation. 10, 70–92. https://doi.org/10.1016/j.gecco.2016.12.005.

Wagner, F.H., Dalagnol, R., Tagle Casapia, X., Streherm, A.S., Phillips, O.L., Gloor, E., Aragão, L.E.O.C., 2020. Regional mapping and spatial distribution analysis of canopy palms in an Amazon forest using deep learning and VHR images. Rem. Sens. 12, 2225. https://doi.org/10.3390/rs12142225.

Wang, S., Zhuang, Q., Lahteenoja, O., Draper, F.C., Cadillo-Quiroz, H., 2018. Potential shift from a carbon sink to a source in Amazonian peatlands under a changing climate. Proc. Natl. Acad. Sci. U.S.A. 115 (49), 12407–12412.